The gas-sensing properties of WO_{3-x} thin films deposited *via* the Atmospheric Pressure Chemical Vapour Deposition (APCVD) of WCl_6 with ethanol

Sobia Ashraf, Christopher S. Blackman*, Simon C. Naisbitt, Ivan P. Parkin
Department of Chemistry, University College London, London, WC1H 0AJ

email: c.blackman@ucl.ac.uk

Abstract

The use of the APCVD reaction of WCl_6 with ethanol to produce tungsten oxide films (3600 – 6700 nm-thick) for use as gas sensors is presented. The response of these films to varying concentrations of ethanol and NO_2 at varying temperatures has been examined. A comparison of the CVD sensors to a thick film (~ 60 mm) screen printed sensor has shown the CVD sensors have a faster rate of response, a stable sensing response and faster return to baseline with no drift at the conditions examined.

Short title

Gas sensing properties of WO_{3-x} thin films deposited *via* APCVD

PACS Codes

81.15.Gh, 07.07.Df

Keywords

CVD, Tungsten Oxide

Introduction

Tungsten oxide (WO_3) has been the subject of extensive investigation since the demonstration of the photochromic and electrochromic properties of amorphous thinfilms by Deb [1]. Thin-films of tungsten oxide can be utilized in different devices such as 'smart windows', anti-dazzle mirrors and information displays [2]. Researchers have tried depositing films for electrochromic studies via a variety of methods including thermal evaporation, sol-gel, spray pyrolysis and pulsed laser deposition [1, 3-5]. CVD methods to tungsten oxide were reviewed by Kirss and Meda and include the use of [WF_6], [$W(CO)_6$], [$W(OC_2H_5)_n$] (where n = 5 or 6) and organometallic tungsten compounds [6]. We have recently demonstrated a new APCVD route to tungsten oxide involving the coreaction of WCl_6 with various oxygen containing solvents [7]. Whilst the electrochromic properties of WO_3 have been well investigated our work has focused on other functional properties of tungsten oxide, such as photochromism, photocatalysis and gas sensing [8, 9]. The mechanism of gas sensing on WO_3 based sensors lies in changes of the oxide film resistance resulting from physisorption, chemisorption and catalytic reactions of gas-phase species at the surface of the film. The sensitivity of the sensor depends upon film parameters such as composition, morphology and microstructure [10]. Recent work has demonstrated that thin-films of tungsten oxide deposited from [$W(OC_6H_6)_6$] via APCVD or from large ionic polyoxotungstate clusters via AACVD make functioning gas sensors [11, 12]. APCVD is a technique that allows for rapid synthesis of films and can produce sensors many times faster than traditional methods used to produce screen-printed sensors. It also has the ability to be scaled such that the simultaneous deposition of hundreds, or thousands, of sensors in a single run and as such is a commercially favourable technique. The current work has focused on examining the properties of APCVD deposited tungsten oxide gas-sensors in more detail, in particular the effect of film thickness on the characteristics of the sensors.

Experimental

APCVD experiments were conducted using a horizontal-bed cold-wall APCVD reactor, which has been described previously [13]. Tungsten hexachloride (99.9%-W) was purchased from Strem Chemicals, Inc. and ethanol (denatured) was purchased from

Aldrich. WCl_6 was placed into a stainless steel bubbler and heated to 240 °C and the vapors generated introduced into the gas stream by passing hot nitrogen gas flowing at 2.0 L/min through the bubbler. Ethanol was loaded into a syringe and was introduced into the plain line gas stream flowing at 10.0 L/min by injection using a variable speed syringe driver to control the total amount introduced and the rate of flow (0.84 cm^3/min). Deposition experiments were conducted by heating the horizontal bed reactor to 625 °C before diverting the nitrogen line through the bubbler and hence to the reactor. At the end of the deposition the bubbler-line was closed and only nitrogen passed over the sensor. The sensor was allowed to cool with the graphite block to ca 150 °C before it was removed. Coated sensors were handled and stored in air. The samples were analysed using X-ray Photoelectron Spectroscopy (XPS), Scanning Electron Microscopy (SEM), Raman spectroscopy and X-ray Diffraction (XRD) by previously described methods [14]. Environmental SEM (ESEM) was used to obtain images of uncoated samples and these were obtained on a Hitachi S-3400N with version 1.20 or the proprietary Hitachi software run in environmental VP-SEM mode with an accelerating voltage of between 10 and 12 kV and a chamber pressure of between 20 and 30 Pa (air).

Gas sensing measurements were carried out using custom-built apparatus, comprising a glass flow-through cell to which three heated devices could be connected and sealed. Gases were applied using computer operated mass flow controllers (Tylan General) through two separate lines. The first carried pre-mixed gases in air of known concentration (100 ppm EtOH, 100 ppm NO_2), purchased directly from source (BOC Special Gases). The remaining line carried dry air (‘zero grade’ compressed air purchased directly from BOC). In this way the gas concentration of the air supplied to the sensors could be controlled (EtOH 1 - 100 ppm; NO_2 5 - 500 ppb). Gas sensing experiments were performed at sensor temperatures between 200 and 600 o C, with the total resistance of the WO_3 film being measured using a digital multimeter (Keithley 175 A). Screen printed sensors were made using an ink composed of tungsten oxide powder (New Metals) and ESL 400 vehicle. 4 layers of ink were printed with intermediate drying steps onto the sensor substrates. The printed layer had a thickness of approximately 60 mm. The sensors

were fired in a furnace at 850°C for 4 hours before being used for the gas-sensing measurements.

Results and discussion

The APCVD reaction of WCl_6 with ethanol depositing onto sensor substrates was examined. Three sets of films were deposited with differing thicknesses, with three repeats at each thickness. Deposition conditions were identical other than the length of deposition, which was varied between 2.5, 5 and 10 minutes. These deposition times gave films with thickness in the electrode gap of approximately 3600, 5400 nm and 6700 nm respectively determined by cross-sectional SEM. The thickness on the electrodes was much reduced relative to the thickness in the electrode gap, in the order of 100s of nanometers, but was not accurately measured. The change in the overall rate of deposition from ~ 1400 nm/min for a 2.5 minute deposition to ~ 700 nm/min for a 10 minute deposition is likely to relate to the fact that WCl_6 is a solid at the bubbler temperatures used and coupled with the relatively high bubbler flow rates this means the WCl_6 is unlikely to be at equilibrium with relation to the vapour above the solid in the bubbler, leading to a high initial rate of vapour transport which will then continue at a lower level for the remainder of the deposition.

The deposited films were blue in colour indicating that they were partially reduced tungsten oxide (WO_{3-x}). WDX analysis gave a composition of $WO_{2.98}$, which indicates partially reduced tungsten oxide with some residual ethanol co-reactant also likely contributing to the value. Chlorine contamination was negligible (<0.1 at. %) although carbon contamination was significant at ~ 7 at. %, which could be present as either graphitic carbon, carbide or adsorbed ethanol. Previous analysis by XPS of similar films deposited on glass showed the carbon to be principally graphitic with a similar level of contamination measured.

A mixture of traditional high-resolution SEM and Environmental SEM was used to examine the films after deposition. The advantage of ESEM is that is allows uncoated samples to be imaged, which whilst being lower resolution than traditional SEM methods

allows the sample to be subsequently analysed for gas response. A typical deposition for a 6700 nm-thick sensor is shown below (figures 1A-D).

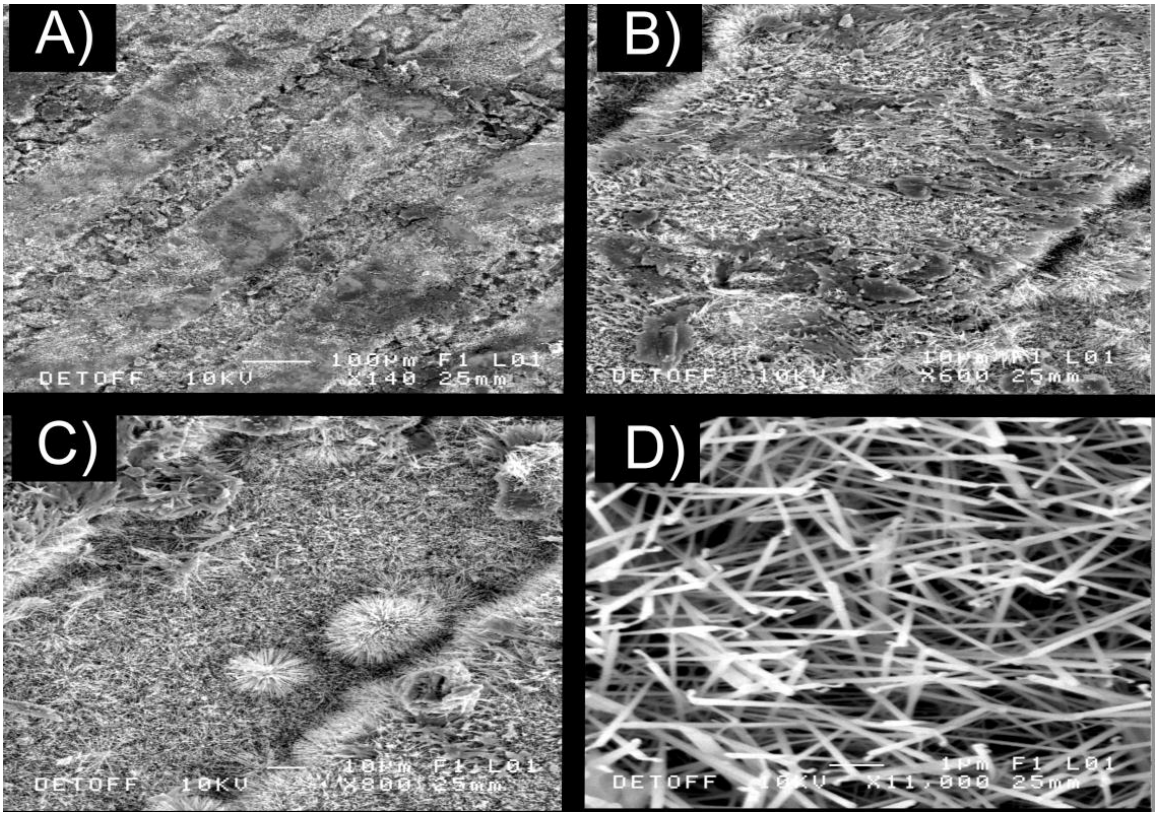

Figure 1:- ESEM image of 6700 nm-thick sensor as-deposited; A) electrode and gap (x140), B) electrode (x600), C) electrode gap (x800), D) electrode gap (x11000).

Figure 1A shows the topography of the sensor. Higher magnification images (figures 1B, 1C) show that the morphology on the electrodes and in the electrode gap are similar with fine, needle-like crystallites. The morphology is most apparent in figure 1D, with the long thin crystallites clearly visible. This morphology is typical of tungsten oxide deposited from WCl_6 and ethanol, seen previously on glass substrates. [11] Whilst this structure would have a high surface area and a highly porous structure, which should be ideal for gas-sensing, it also has poor connectivity between grains which is likely to lead to a high resistance across the electrode gap. These morphologies are very similar to those seen previously for tungsten oxide thin films when deposited from the single-source precursor

tungsten(VI) hexaphenoxide but only when deposited under the influence of an electric field. [10] Thinner films (3600, 5400 nm) had identical morphology although coverage of the electrodes was less.

Environmental SEM was used to examine the films after their use as sensors (figures 2A-D).

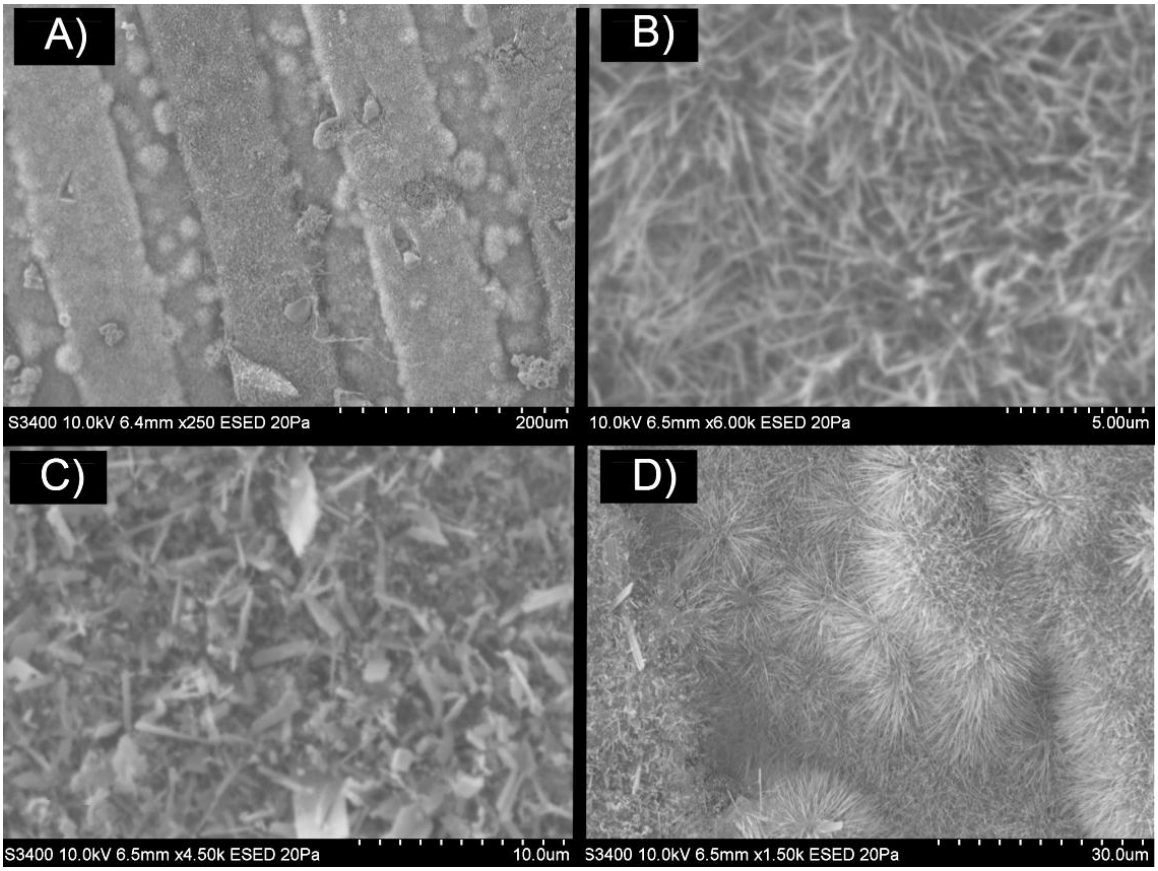

Figure 2:- ESEM image of 6700 nm-thick sensor after gas-sensing; A) electrode and gap (x250), B) 'light' electrode (x6000), C) 'dark' electrode (x4500), D) electrode-gap (x1500).

In figure 2A it is apparent that the interdigitated electrodes appear different under the electron microscope with one 'light' and one 'dark' electrode, in figure 2A the furthest left-hand electrode is the 'light' electrode with the next one being the 'dark' electrode, and these alternate, in other words the positive and negative electrodes appeared different

under the electron microscope. In fact this difference was easily observed under an optical microscope and was even visible to the naked eye on certain samples.

The light electrode shown in figure 2B has an almost identical structure to that seen on the as-deposited electrodes (figure 1D). This is in itself surprising; previous results have shown similar structure thinner films on glass are microstructurally thermally unstable at the uppermost operating temperatures used for these gas-sensors. [7] However the dark electrode (figure 2C) has a different structure to the material on both the as-deposited and light (after gas-sensing) electrodes. On the dark electrode most of the fine needle-like structures have collapsed and coalesced into larger rectangular or cube-like structures, although some needles do remain, with some underlying micro-crystalline material of spherical form.

The image of the electrode-gap of a 6700 nm-thick sensor after gas-sensing (figure 2D) appears to have an almost unchanged microstructure from the sensor as-deposited (figure 1C). This indicates that the as-deposited film morphology is thermally stable for a 6700 nm-thick sensor. The morphology is also similar to that seen for the ‘light’ electrode after use (figure 2B).

However, the results for thinner films were strikingly different (figures 3A-D).

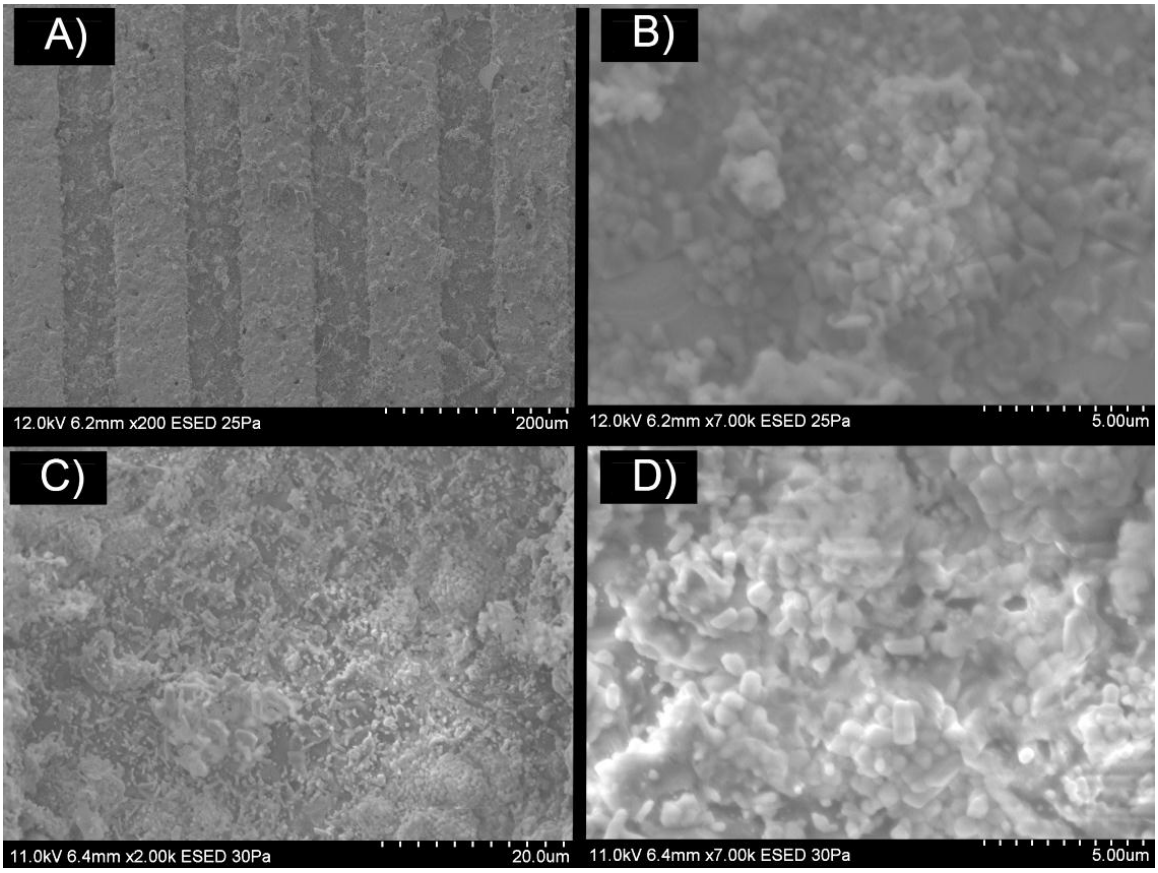

Figure 3:- ESEM image of 3600 nm-thick sensor after gas-sensing; A) electrode and electrode-gap (x200), B) electrode (x7000), C) electrode-gap (x2000), D) electrode-gap (x7000).

Looking at an overview of the electrodes (figure 3A) there is no obvious contrast between alternating electrodes. In fact the structure on the electrodes was identical and it can be seen that the electrode (figure 3B) of the 3600 nm-thick film after gas-sensing appears different to either the 'light' (figure 2B) or 'dark' (figure 2C) electrodes of a 6700 nm-thick film. It again shows a collapse of the fine needle-like structure but rather than forming grains and rectangular crystallites it is entirely composed of an agglomeration of larger rounded crystallites, which has parallels to the underlying microcrystalline material seen on the dark electrode of a 6700 nm-thick sensor (figure 2C). Examination of the electrode-gap (figure 3C) compared with that found on a thicker sensor (figure 2D) highlights the structural differences and a magnification of the electrode-gap (figure 3D) shows the total loss of the needle-like structure found before testing, the appearance

being similar to the material on the electrode (figure 3B). This shows that the needle-like tungsten oxide morphology deposited on the gas-sensors is thermally unstable below a certain thickness. In fact the sensors of intermediate thickness (5400 nm) were somewhere between the two structures in terms of morphology. They displayed obvious light and dark contrast between the electrodes and the needle-like as-deposited morphology had largely coalesced forming predominantly rectangular crystallites, although there were clusters of small cubic crystallites (figure 4).

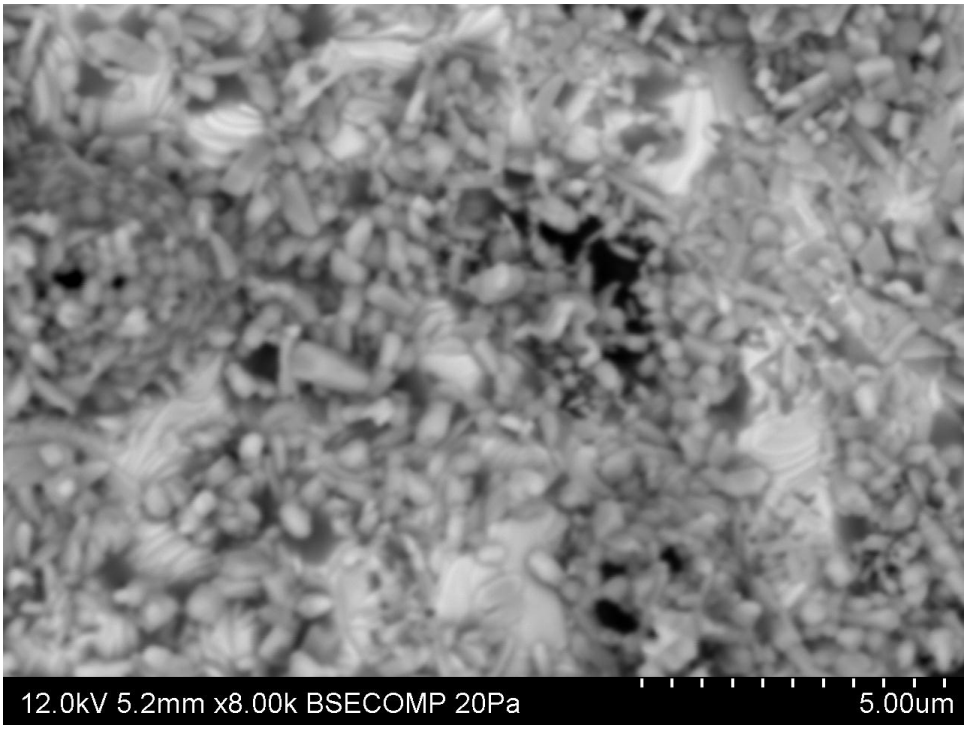

Figure 4:- ESEM image of 5400 nm-thick sensor after gas-sensing; 'light' electrode (x8000).

The sensors were also analysed using X-ray Diffraction (figure 5) and Raman spectroscopy before and after use for gas-sensing (figure 6).

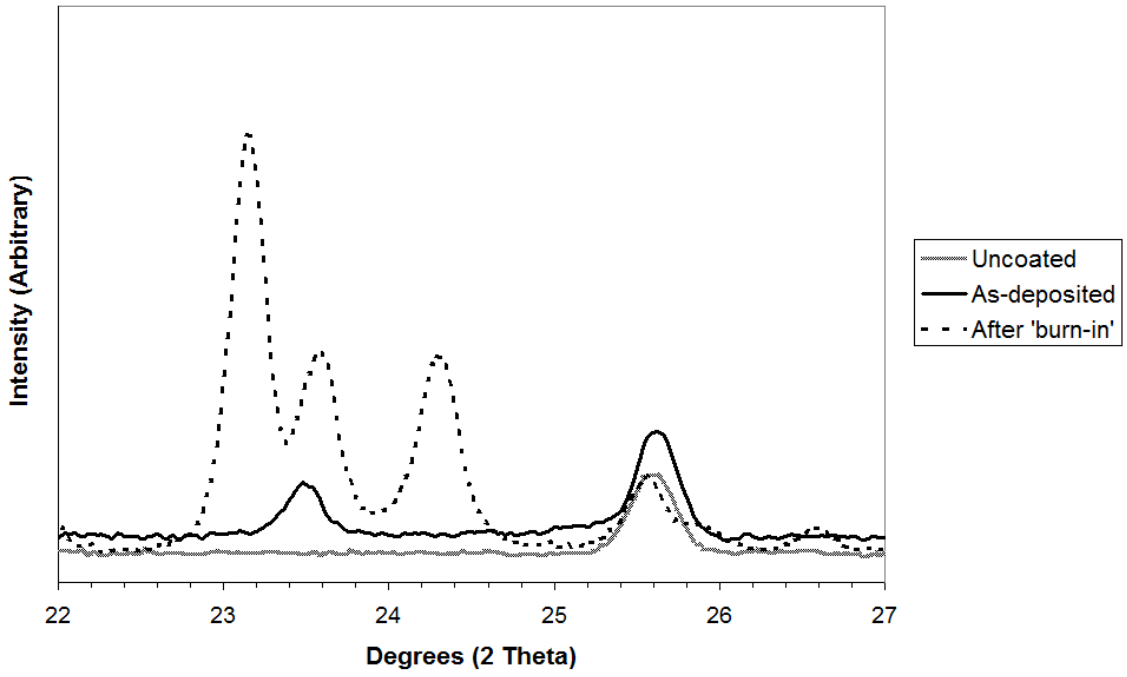

Figure 5:- XRD pattern of uncoated and 6700 nm-thick coated gas-sensor before (as-deposited) and after use (burn-in).

The X-ray Diffraction patterns (figure 5) are displayed between 22 and 27 ° 2θ, which is the area in which the most intense peaks of monoclinic tungsten oxide are observed. The uncoated substrate has one peak in this region at 25.6 ° 2θ, which is apparent in all the patterns, and corresponds to aluminium oxide from the sensor substrate. The XRD pattern of the as-deposited film has only one other diffraction peak in this region at ~ 23.5 ° 2θ, which corresponds to the [010] diffraction peak of monoclinic tungsten oxide. This lone diffraction peak is observed in preferentially oriented films of partially reduced tungsten oxide and is associated with the needle-like morphology observed in figure 1, with the presence of partially reduced tungsten oxide consistent with the WDX analysis results. [7] After the sensor has been used the XRD pattern is consistent with the formation of oxidized randomly oriented monoclinic tungsten oxide. [13] The oxidation of the film from partially reduced to fully oxidized tungsten oxide is to be expected in a sensor run at temperatures up to 600 °C in air.

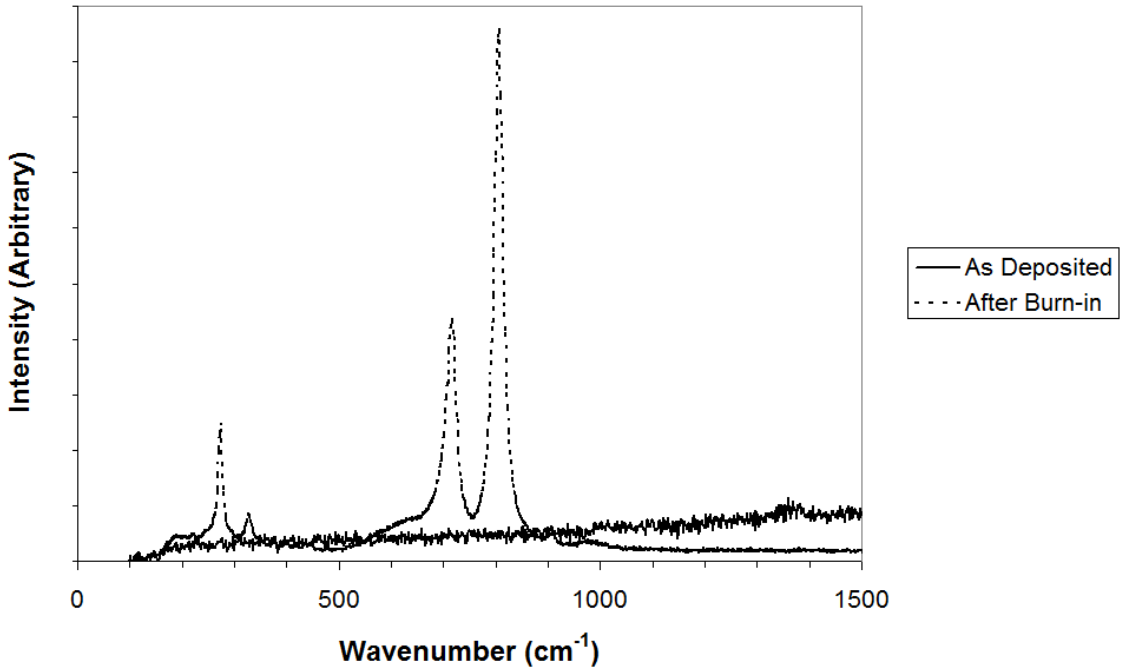

Figure 6:- Raman spectra of 6700 nm-thick coated gas-sensor before (as-deposited) and after use (burn-in).

It was found that the as-deposited films gave no Raman spectrum (figure 6), which is possibly due to the fact that the partially reduced form of tungsten oxide has previously been found to be a relatively weak Raman scatterer. After use the films gave the Raman pattern expected for crystalline fully oxidized tungsten(VI) oxide. [7, 14] These observations confirm the results from XRD that the initially partially reduced tungsten oxide is fully oxidized when the sensor is in use,

The gas sensing results for a 3600 nm-thick sensor are shown below. In all cases for a single-gas response measurement the gas pulse occurred at 1800 seconds. Due to the particular equipment used the gas pulse may be measured between 1798 and 1805 seconds on any one run. It can be seen in figure 7 that there is a difference in the shape of the sensor response when measured at 500 °C and 400 °C. At 400 °C it appears as though the steady state response has not been reached, whereas at 500 °C it has. In fact all measurements made below 500 °C show a non-steady state sensor response.

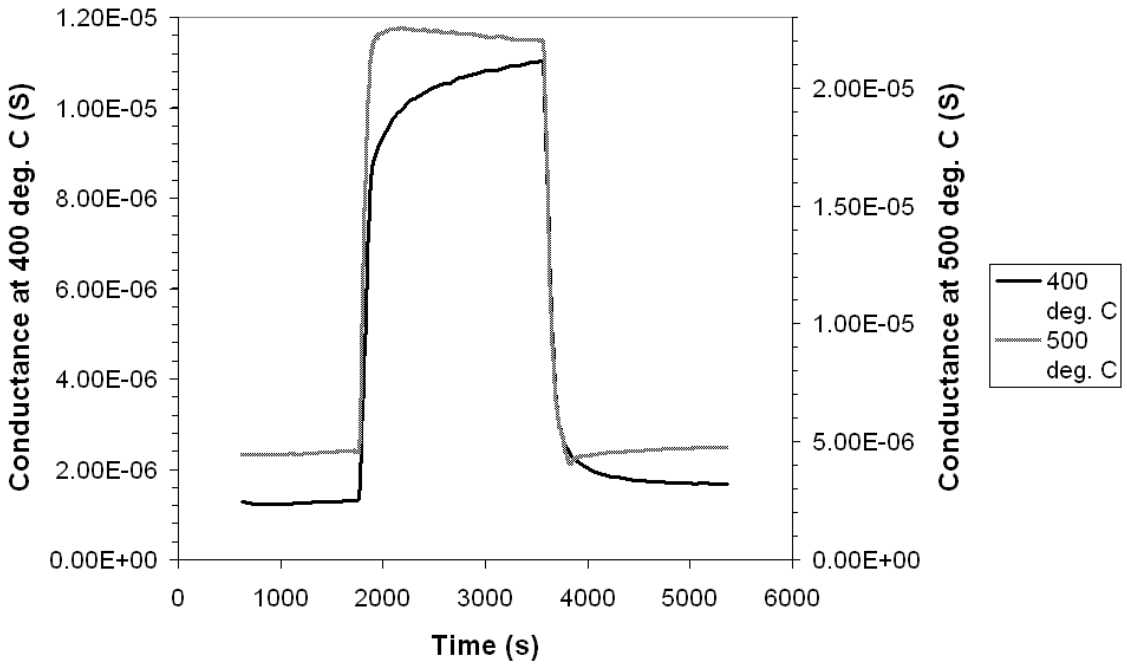

Figure 7:- Sensor response for a 3600 nm-thick sensor to 20 ppm ethanol at 400 and 500 ℃.

The response, defined as the baseline resistance taken just before the test gas was admitted to the cell divided by the sensing resistance taken at the end of the gas exposure for a material exhibiting an n-type response to a reducing gas, to 20 ppm ethanol increases from 2.50 at 300 °C up to 8.34 at 400 °C decreasing thereafter to 4.86 at 500 °C (figure 8). The peak operating temperature for the sensor therefore lies between 350 and

450 °C.

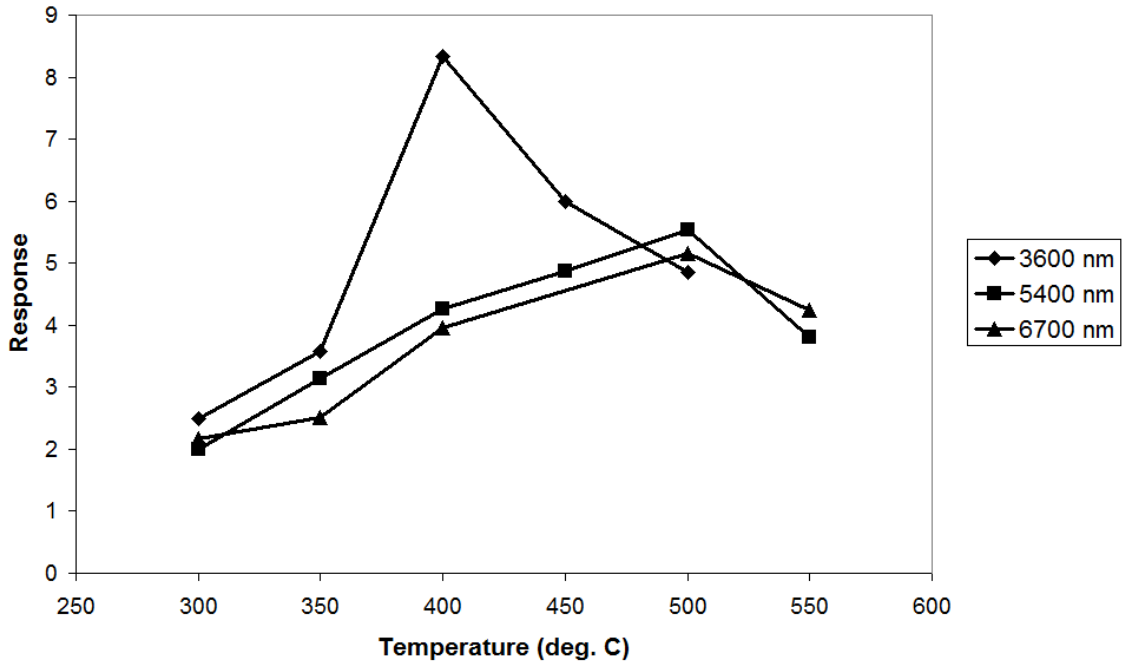

Figure 8:- Sensor response to 20 ppm ethanol at a given operating temperature for a sensor of given thickness.

During sensing there are expected to be two competing factors. At lower temperatures the response is slower and the steady state response is not achieved. At higher temperatures the reactions at the surface will proceed at an increased rate and will attain equilibrium more quickly but the reaction will affect the conductivity to a lesser degree due to the higher number of conduction carriers present in the material at elevated temperature. The balance between these two factors could lead to the peak operating temperature observed.

During testing the baseline conductance increases with increasing temperature. This change in resistance is consistent with the thermal change in resistance associated with a semiconductor. The change in baseline resistance was plotted as an Arrhenius plot (figure 9).

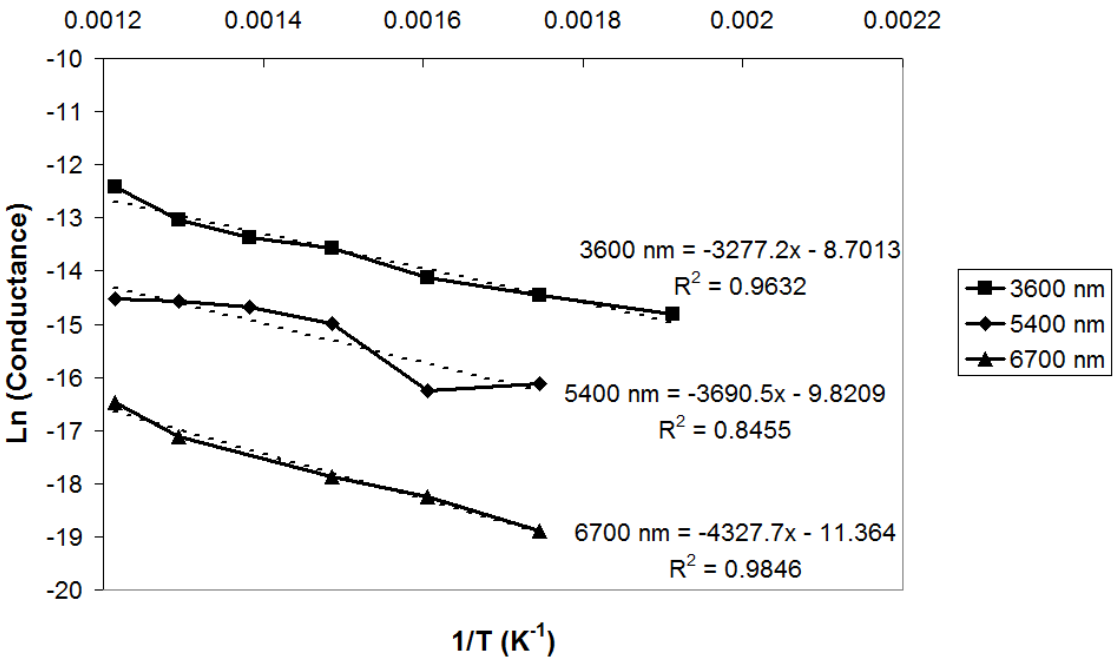

Figure 9:- Arrhenius plot of baseline resistance for sensors of a given thickness.

The activation energy calculated from the baseline resistance using this method yields a value of 0.282 eV. This value is similar to that seen for previous tungsten oxide gas sensors of 0.15 – 0.35 eV [15] and 0.19 – 0.42 eV [16].

Subsequently the sensors were analysed for extended period of times to determine the sensor periodic stability. The sensor was analysed at 400 °C and was exposed to 20 ppm ethanol (figure 10).

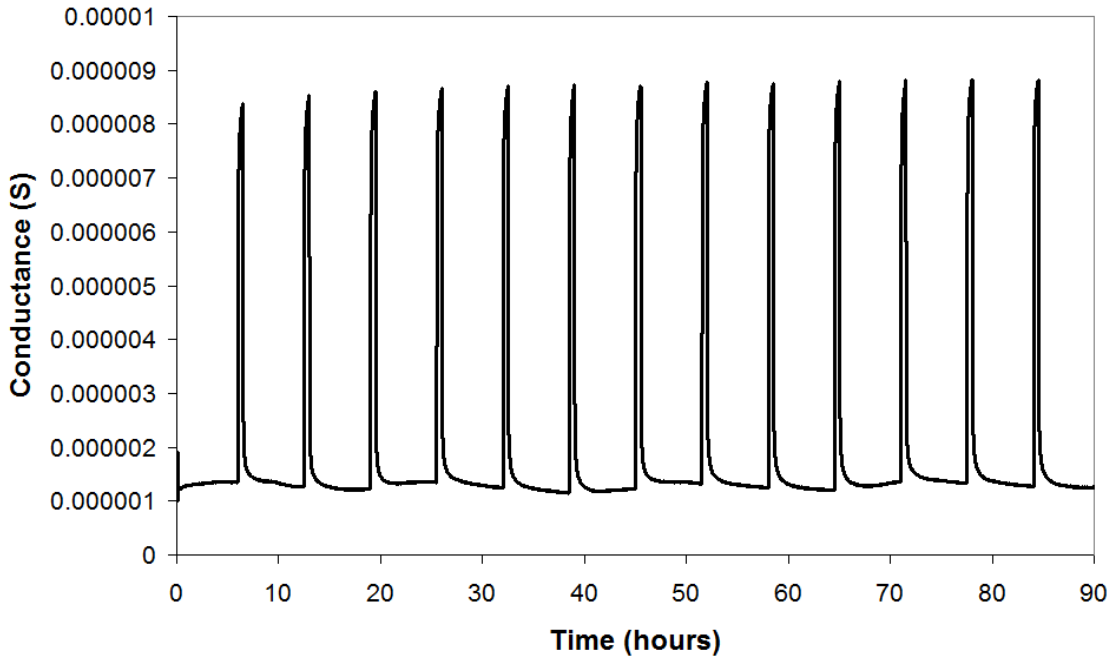

Figure 10:- Periodic stability for a 3600 nm-thick sensor to 20 ppm ethanol at 400 ℃.

The data shows that the sensor has both a stable sensing resistance and stable baseline resistance over the test period. The variation of the baseline is periodic and varies slightly over a 24 hour cycle. Therefore these variations are attributed to environmental changes in the laboratory.

The sensors were exposed to varying concentrations of ethanol at a temperature of 400 °C and the response measured (figure 11).

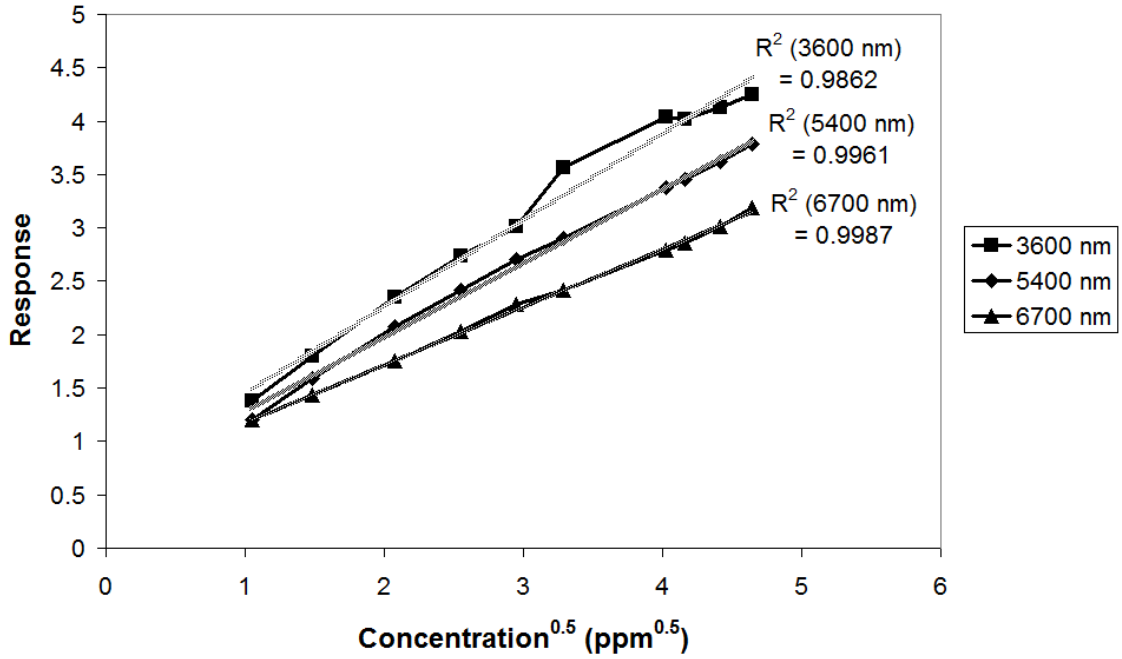

Figure 11:- Response vs. [ethanol]$^{0.5}$ at 400 °C for a sensor of given thickness.

The response curve is linear to the square root of the ethanol concentration. This is a common observation in the responses of other gas-sensing metal oxides to a variety of gases. [17, 18] Although the value of the exponent applied to the concentration is commonly attributed directly to the different oxygen species at the sensor surface that are proposed to mediate the sensor response recent work has shown that it may, in fact, be due to microstructure. [10, 19]

The sensing results for the 5 minute deposition (5400 nm-thick) are discussed below.

A steady state response was reached for a 5400 nm-thick sensor as low as 300 °C, whereas the thinner 3600 nm sensors only reached a steady state at 550 °C. The response to 20 ppm ethanol at 300 °C is 1.99 which increases to a maximum response of 5.53 at 500 °C and subsequently decreases to 3.80 at 550 °C. This peak response is recorded at a higher temperature than seen for the thinner sensors deposited over 2.5 minutes. The response at all temperatures below the peak temperature (500 °C) is lower for a 5400 nm-thick sensors than for the equivalent response for a 3600 nm-thick sensor. Baseline

resistance ranges from 1 x 10^7 Ω at 300 °C to 2 x 10^6 Ω at 550 °C, which is to be expected for a semiconductor. The baseline resistance at 300 °C for a 5400 nm-thick sensor (1 x 10^7 Ω) is far higher than the 8 x 10^5 Ω recorded for a 3600 nm-thick sensor, which shows that the sensor resistance increases with thickness. Increasing film thickness is normally correlated with increased conductivity and therefore reduced resistance, through the increase in cross-sectional area. However the opposite trend is observed here. An Arrhenius plot was made of the response data at various temperatures (figure 9) and the activation energy calculated from the baseline resistance using this method yields a value of 0.317 eV. This value is greater than found (0.282 eV) for the 3600 nm-thick sensor. This increase in activation energy for conduction with increasing thickness indicates that the trend in increasing resistance with thickness is due to greater difficulty of conduction through the material in the thicker sensor.

Subsequently the sensors were analysed for the sensor response and baseline stability by periodically cycling the sensor over ~ 100 hours. The data showed that the sensors had both a stable sensing resistance and stable baseline resistance over the test period.

The sensors were exposed to varying concentrations of ethanol at a temperature of 400 °C and the response measured (figure 11).

The sensor response for a 5400 nm-thick sensor at 400 °C was consistently lower than the equivalent sensor response recorded on the thinner 3600 nm-thick sensor. A plot of the response against concentration is not linear but has an identical form to the thinner sensor when exposed to ethanol. These data were plotted as a chart of response against the square root of the ethanol concentration (figure 11) and the response curve found to be a good fit (R^2 = 0.9961) for a linear relationship between the square root of the ethanol concentration and the response. This is similar to the results seen for the thinner 3600 nm sensors.

The sensing results for the 6700 nm-thick sensors are shown in figure 8 and figure 11.

At temperatures below 400 °C the data showed that no steady state response was achieved during the period of sensor exposure examined. This is contrary to that found

for a 5400 nm-thick sensor where a steady state was achieved even at 300 °C but similar to that seen for a 3700 nm sensor, although the temperature at which the steady state response was first observed was 100 °C higher (500 °C) for the thinner sensors. Baseline resistance varied from 1.2 x 10^8 Ω at 300 °C to 1.3 x 10^7 Ω at 550 °C, which is consistent for the change in resistance with increasing temperature observed for a semiconductor.

An Arrhenius plot was made of the response data at various temperatures (figure 9) and used to determine the activation energy, which gave a value of 0.373 eV which is higher than that observed for either the 3600 nm-thick sensor (0.282 eV) or 5400 nm sensor (0.317 eV) and again shows a trend for increasing calculated activation energy with increasing sensor thickness. Also the baseline resistance for a 6700 nm-thick sensor at all temperatures was higher than the equivalent resistance for a 5400 nm-thick sensor demonstrating that the sensor resistance increases with increasing thickness. The microstructure evident in figure 2D shows that the needle-like structure is retained after sensor conditioning whereas the needles originally present in the 3600 nm-thick sensor have collapsed and merged (figures 3C and 3D). The higher baseline resistance and activation energy for the thicker sensors may be attributable to a higher proportion of relatively poorly conducting particle boundaries between needles in the electrode gap acting to hinder effective conduction between neighbouring grains compared to more coherent grain boundaries in the collapsed structure present in the 3600 nm-thick film. However the range of film thickness examined is narrow and it would be necessary to extend this to categorically demonstrate the increase in activation energy with film thickness.

The sensors were analysed for the sensor periodic stability and as seen for the thinner sensors the longer term stability of the 6700 nm-thick sensors is good with both baseline and sensing conductance values consistent over the analysis period.

The response to varying concentrations of ethanol demonstrate that the as the WO_3 sensing layer becomes thicker the lower the response, with the values for the 6700 nm-thick sensor being lower than the equivalent values seen for 5400 nm or 3700 nm-thick sensors. It would be expected that the needle-like morphology that is maintained in the

thicker sensors after conditioning (figure 2D) would give a higher surface area to bulk volume ratio than the collapsed structure than seen in the thinner sensors (figures 3C and 3D). This should mean that the thicker sensors have greater capacity for conductance changing reactions and therefore a higher response. One reason for this trend being reversed could be if the underlying microstructure in the electrode gap of the thicker sensors has collapsed as seen for the 3600 nm-thick sensors and there are lots of the needle-like structures above this more compact material where the ethanol tends to combust before it can react on the surface in conductance changing reactions. Another explanation could be that the needle structure will have a different composition of surface to bulk and grain and particle boundaries, being particularly high in low coherency particle boundaries. These particle boundaries may be less gas sensitive than the grain boundaries of higher coherency that are present in the collapsed structure of the thinner sensor. It may also be that the particle boundaries hinder conductivity through the thicker films and this tends to increase resistance and reduce sensitivity since there are fewer and more difficult pathways for the conduction species across low coherency boundaries. This is corroborated by the higher activation energies in the thicker films although also subject to the same caveat regarding the film thickness range examined.

As seen for thinner sensors it was apparent from a plot of response against the square root of the ethanol concentration (figure 11) that the sensor response was linear ($R^2 = 0.9987$) to the square root of the ethanol concentration over the concentration range examined (1.1 – 21.6 ppm).

A comparison was made between a 6700 nm-thick sensor and a 60 μm-thick screen printed sensor, chosen because this is the typical thickness for a commercial screen printed sensor. The operating conditions chosen were the optimum operating conditions for the screen-printed sensor examined in the test. The gas-sensing properties were recorded using analysis equipment capable of improved temporal resolution to that used for the previous measurements, measuring the resistance several times a second to allow a comparison of rate of response between the CVD sensor and the screen printed sensor. The test was carried out at 400 °C with an ethanol concentration of 20 ppm.

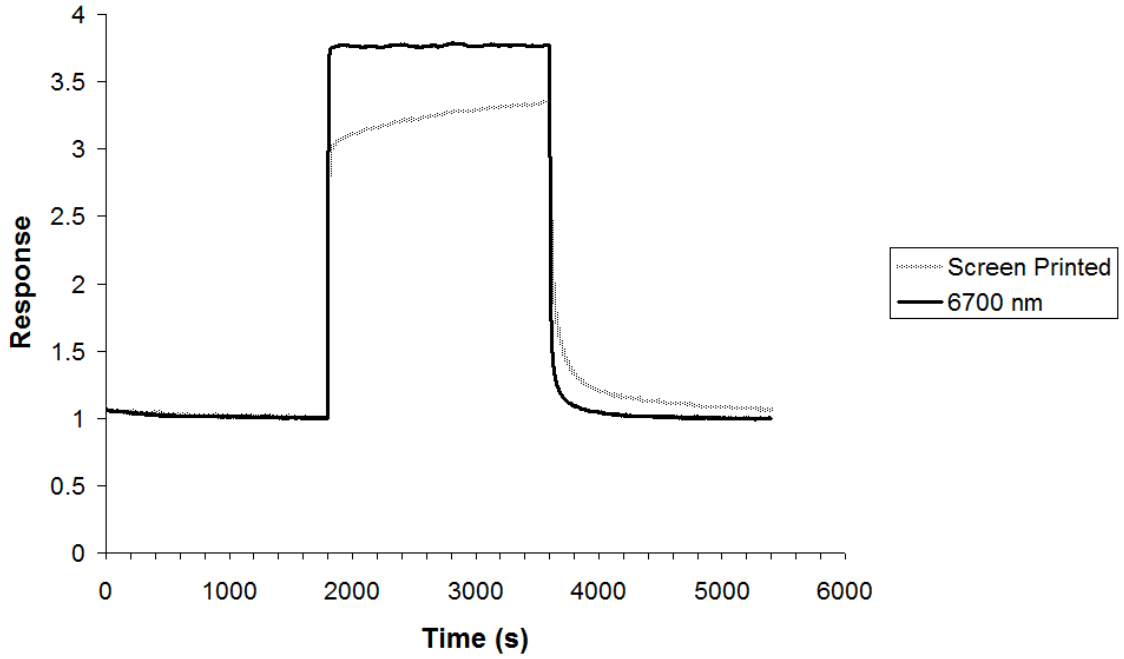

Figure 12:- Comparison of sensor response to 20 ppm ethanol between a screen printed sensor and a 6700 nm-thick CVD sensor, both at 400 °C.

It is apparent in figure 12 that the 6700 nm-thick screen printed sensor gives a higher response to 20 ppm ethanol at an operating temperature of 400 °C, although the values are not significantly different. More importantly however it is apparent that the maximum response is reached almost immediately, whereas the response of the screen printed sensor does not stabilise during the measurement period. It should also be noted that the CVD sensor displays improved desorbtion of the test gas, returning more rapidly to the initial resistance, whereas the screen printed sensor returns slowly and incompletely to the initial value. An expansion of the initial region of the sensor response is shown in figure 13.

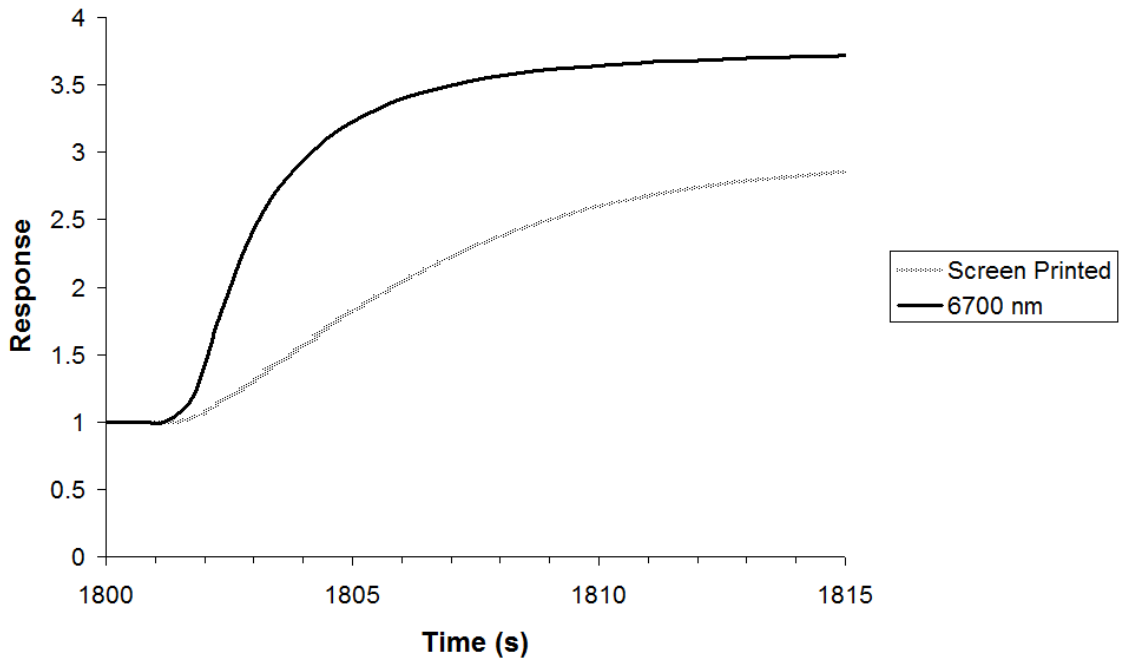

Figure 13:- Comparison of rate of sensor response to 20 ppm ethanol between a screen printed sensor and a 6700 nm-thick CVD sensor, both at 400 ℃.

It is clear from figure 13 that a further advantage the CVD sensor has a significant advantage over the screen printed sensor since the initial rate of sensor response is increased with the CVD sensor responding more rapidly to the incident gas. In fact for the CVD gas sensor the final sensor response is almost achieved within 10 seconds of gas exposure as opposed to not being finished in 1800 seconds for the screen printed sensor

Tungsten oxide is more commonly used to sense oxidizing gases such as NO_2 or O_3 than reducing gases such as ethanol, therefore a series of tests were carried out exposing the sensors to both 200 ppb and varying concentrations of NO_2.

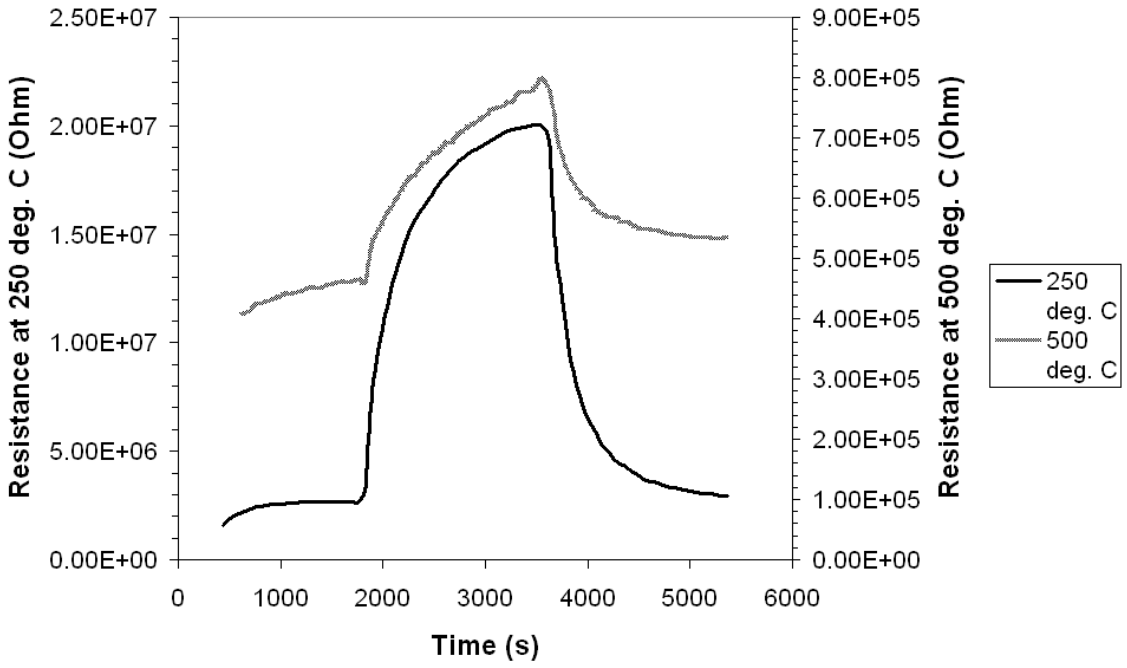

Figure 14:- Sensor response for a 3600 nm-thick sensor to 200 ppb NO_2 at 250 and 500 ℃.

The graphs of response for NO_2 at both low and high sensor operating temperature (figure 14) have a different form to that of ethanol at either low or high (figure 7) temperatures. The response graph has a less rapid initial rate of response and a stable sensing response is not reached at any of the operating temperatures examined. The shape of the response curves changes with temperature. Those at lower temperature have a larger initial fast response as a fraction of the total response and appear to almost reach a saturated response. The response, defined as the sensing resistance divided by the baseline resistance for a p-type response to an oxidizing gas, to 2 ppm NO_2 is a maximum at the lowest operating temperature measured (250 °C) and decreases at increasingly higher temperatures (table 1).

Operation Temperature (° C)	Sensor Response
250	7.40

300	5.24
350	3.85
400	2.33
450	2.12
500	1.73
550	1.22

Table 1:- Sensor response to 200 ppb NO_2 at a given operating temperature for a 3600 nm-thick sensor.

One of the gas sensors was then exposed to varying concentrations of NO_2 at a (non-optimum) temperature of 400 °C (figure 15).

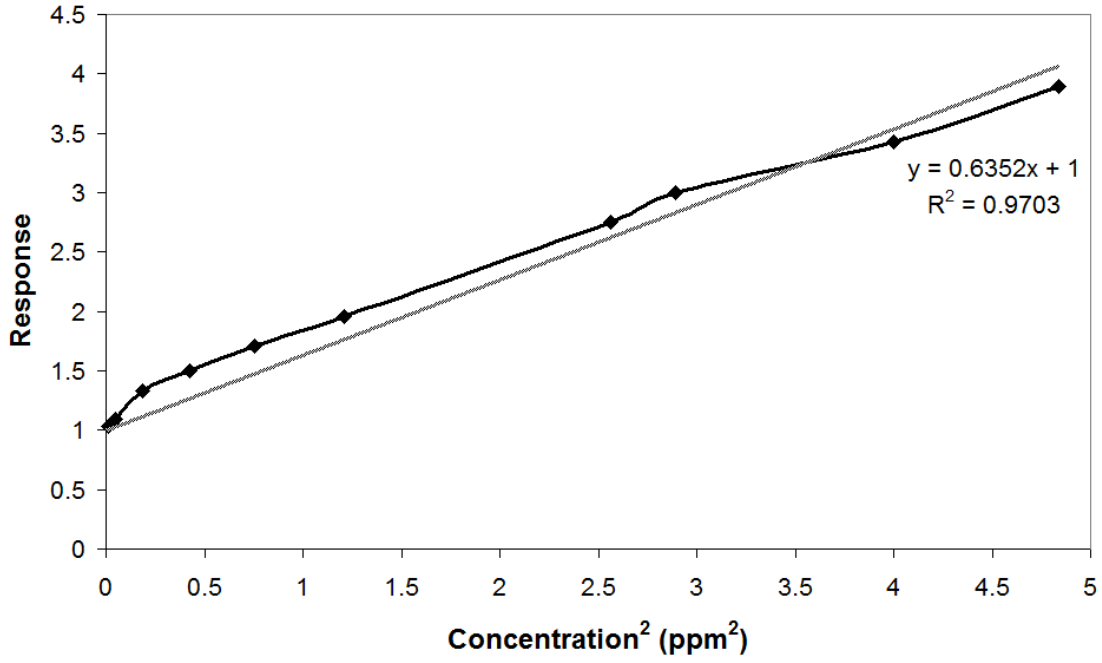

Figure 15:- Response vs. $[NO_2]^2$ at 400 °C for a 3600 nm-thick sensor.

The response curve is linear to the square of the NO_2 concentration. Again the value of the exponent of the concentration may relate to the surface oxygen species that mediate the sensor response, hence the exponent for NO_2 is different to that for ethanol.

Conclusions

The APCVD reaction of WCl_6 and ethanol has been used to produce thin film (3600 – 6700 nm-thick) tungsten oxide gas sensors on pre-patterned interdigitated electrodes. As deposited the films are partially reduced and have a needle-like morphology and a preferred crystallographic orientation relative to the substrate along the <010> plane. Upon conditioning the tungsten oxide is fully oxidized; the thinnest films were morphologically unstable with the needle-like structure being replaced by an agglomeration of rounded crystallites however the thickest films retained the needle-like morphology. The sensors were exposed to varying concentrations of ethanol and NO_2 and the sensor response examined. It was found that the baseline resistance of the sensors increased with increasing thickness which was attributed to the changes in microstructure upon use between thick and thin sensors. This effect was also observed in the difference between the activation energies of conductance between thick and thin sensors. The greatest response to ethanol was recorded for the thinnest film sensors, with a value greater than 8 for 20 ppm ethanol in dry air at 400 °C. The periodic sensors stability was found to be good with excellent reproducibility of sensing resistance and recovery to baseline over extended test times. The sensors response to varying concentrations of ethanol was found to be linear to the square root of the ethanol concentration over greater than one order of magnitude. A direct comparison with a thick film screen printed tungsten oxide sensor (~ 60 μm) showed that the response of the thin film CVD sensors was higher, with a faster rate of response also achieving a stable sensing response. The CVD sensors also displayed a faster return to baseline after response and no appreciable drift unlike the screen printed sensor. Tests carried out with CVD thin film sensors to part-per-billion concentrations of NO_2 showed the films were sensitive to NO_2 even at relatively low temperatures with the response proportional to the NO_2 concentration squared.

Acknowledgements

The EPSRC is thanked for providing the grant for this work. Dr Keith Pratt of City Technology is thanked for useful discussions. Mr. Kevin Reeves of UCL Archaeology is thanked for assistance with SEM and techniques. I.P.P. thanks the Royal Society/Wolfson Trust for a merit award.

References

[1] Deb, S K 1973 Optical and photoelectric properties and colour centres in thin films of tungsten oxide *Philos. Mag.* **27** 801

[2] Monk P M S, Mortimer R J and Rosseinsky D R 1995 *Electrochromism: Fundamentals and Applications* (VCH New York)

[3] Cantalini C, Atashbar M Z, Li Y, Ghantasala M K, Santucci S, Wlodarski W and Passacantando M J 1999 Characterization of sol-gel prepared WO_3 thin films as a gas sensor *J. Vac. Sci. Technol. A* **17** 1873

[4] Regragui M, Addou M, Outzourhit A, Bernede J C, El Iddrissi E L B, Benseddik E and Kachouane A 2000 Preparation and characterization of pyrolytic spray deposited electrochromic tungsten trioxide films *Thin Solid Films* **358** 40

[5] Rougier A, Portemer F, Quede A and El Marssi M 1999 Characterization of pulsed laser deposited WO_3 thin films for electrochromic devices *Appl. Surf. Sci.* **153** 1

[6] Kirss R U and Meda L 1998 Chemical vapor deposition of tungsten oxide *Appl. Organometallic Chem.* **12** 155

[7] Blackman C S and Parkin I P 2005 Atmospheric pressure chemical vapour deposition of crystalline monocline WO_3 and WO_{3-x} thin films from reaction of WCl_6 with O-containing solvents and their photochromic and electrochromic properties *Chem. Mater.* **17** 1583

[8] Granqvist C G 1995 *Handbook of Inorganic Electrochromic Materials* (Elsevier New York)

[9] Granqvist C G 2000 Electrochromic tungsten oxide films: Review of progress *Sol. Energy. Mater. Sol. Cells* **60** 201

[10] Naisbitt S C, Pratt K F E, Williams D E and Parkin I P 2006 A microstructural model of semiconducting gas sensor response: The effects of sintering temperature on the response of chromium titanate (CTO) to carbon monoxide *Sens. Actuators, B, Chem.* **114** 969
[11] Shaw G, Parkin I P, Pratt K F E and Williams D E 2005 Control of semiconducting oxide gas-sensor microstructure by application of an electric field during aerosol-assisted chemical vapour deposition *J. Mater. Chem.* **15** 149
[12] Ashraf S, Blackman C S, Palgrave R G and Parkin I P 2007 Aerosol-assisted chemical vapour deposition of WO_3 thin films using polyoxometallate precursors and their gas sensing properties *J. Mater. Chem.* **17** 1063
[13] Blackman C, Hyett G and Parkin I P 2007 The effect of oxygen-containing reagents on the crystal morphology and orientation in tungsten oxide thin films deposited via atmospheric pressure chemical vapour deposition (APCVD) on glass substrates *Faraday Discussions* **136** 329
[14] Salje E 1975 Lattice dynamics of WO_3 *Acta Crystallogr.* **A31** 360
[15] De Giulio M, Manno D, Micocci G, Serra A and Tepore A 1997 Gas-sensing properties of sputtered thin films of tungsten oxide *J. Phys. D: Appl. Phys.* **30** 3211
[16] Aguir K, Lemire C and Lollman D B B 2002 Electrical properties of reactively sputtered WO_3 thin films as ozone gas sensor *Sens. Actuators, B Chem* **84** 1
[17] Barsan N, Schwizer-Berberich M and Gopel W 1999 Fundamental and practical aspects in the design of nanoscaled SnO2 gas sensors: a status report *Fresenius J. Anal. Chem.* **365** 287
[18] Williams D E 1987 *Solid State Gas Sensors* ed P.T. Mosley and B.C. Tofield (IOP Publishing Bristol)
[19] Windischmann H and Mark P 1979 A Model for the Operation of a Thin-Film SnOx Conductance-Modulation Carbon Monoxide Sensor *J. Electrochem Soc.* **126** 627